Journal of Corrosion and Materials
www.corromat.com

J. Corros. Mater. (2023) 2(2), 113–127.

Interface Integrity and Degradation-Sensitive Failure Pathways in AA2319 Aluminium Wire Direct Energy Deposition on 2xxx and 6xxx Substrates

John B. Goodenough[1,*], Liam MacDonald[2]

[1] *Walker Department of Mechanical Engineering, The University of Texas at Austin, Austin, Texas 78712-1591, USA*

[2] *Department of Mechanical Engineering, Price Faculty of Engineering, University of Manitoba, Winnipeg, Manitoba R3T 5V6, Canada.*

[*] Corresponding author: jgoodenough@mail.utexas.edu

[2] liammacdonald211@gmail.com

(Received: 18 August 2023. Received in revised form: 21 October 2023. Accepted: 7 November 2023. Published online: 30 December 2023.)

Abstract

The retained-substrate aluminium wire direct energy deposition process produces a thin mechanically active interlayer where the substrate heat affected zone, partly molten metal, fusion zone, first deposited layer, and top AA2319 deposit take load through distinct mechanisms. The aim of this paper is to investigate AA2319 deposits deposited on 2219-T8, 2024-T3, conventional rolling 6061-T6, and rapid solidification 6061-T6 substrates in as-deposited, inter-pass rolling, heat treatment, and rolling and heat treatment states. The issue to be addressed was whether retained interface performance was dominated by chemical compatibility, local hardening, sensitivity of first layer defects, or substrate side heat affected zone softening. Factors taken into consideration were tensile behavior, microhardness distribution, optical microscopy, SEM fractography, EDS composition analysis, and digital image correlation. 2219+2319 couple demonstrated the best compatibility of the alloys. In the as-deposited state, the proof stress was 118 $\pm$ 8 MPa, ultimate tensile strength was 257 $\pm$ 13 MPa, and elongation was 8.5 $\pm$ 1.5% elongation, indicating that the softer AA2319 deposit controlled the tensile response. Inter-pass rolling increased the proof stress to 224 $\pm$ 21 MPa, whereas elongation was lowered to 2.2 $\pm$ 0.7%. It indicated that deformational strengthening alone failed to confer the damage tolerance of the lower wall. The highest strength coupled with inter-face-tolerance was observed in the case of the rolled-then-heat-treated 2219+2319 combination with 272 $\pm$ 22 MPa of proof stress and 362 $\pm$ 26 MPa of ultimate tensile strength, and without failure at the fusion line. In the 2024+2319 interface, however, magnesium alloy dilution of the lower portion increased the fusion zone hardness to about 99 HV. Yet due to low elongation and sensitivity to grain-boundary cracking, the lower deposited portion remained less desirable. Softened heat-affected zones on the substrate side of 6061 interface dictated performance, rather than cracking within the lower deposit, as was seen for other substrates. Quickly-solidified 6061 provided better results in terms of strength and uniformity of strain following heat treatment compared to normally-rolled 6061. Direct corrosion data could not be obtained; thus, any corrosion analysis was limited to mechanical- and chemical-vulnerable regions.

Keywords: aluminium alloys; AA2319; wire direct energy deposition; WAAM; retained substrate; fusion boundary; heat-affected zone; inter-pass rolling; microhardness; digital image correlation; localized degradation.

1. Introduction

These materials are highly significant for structural applications due to their light weight and mechanical properties. General aluminum-alloy handbooks describe their broad use and corrosion-relevant surface behavior [1]. Aircraft applications show why modern aluminum alloys remain important in weight-sensitive structural design [2]. Light-alloy metallurgy further shows that mechanical response depends on solute state, precipitate morphology, grain structure, intermetallic compounds, stress state, and heat treatment [3]. These aspects become particularly important when aluminium alloys are joined through fusion processes such as welding or arc-based additive manufacturing [4]. Such processes can involve dissolution, coarsening, redistribution of strengthening precipitates, partially molten zones, pores, oxides, and compositional inhomogeneity [5].

The wire version of DED, which includes wire and arc additive manufacturing (WAAM), provides fast deposition speed, efficient use of feedstock, and applicability to large near-net-shape aluminium components [6]. Process-development studies also show the importance of shielding and deposition control in wire arc additive manufacture [7]. Design-oriented WAAM studies describe stiffening, wall-type, repair, boss-type, hybrid, and other build features that can reduce the need for machining from plate or bar stock [8]. Reviews of aluminium WAAM emphasize that build efficiency must be considered together with microstructure and defect control [9]. Broader additive-manufacturing literature connects process route, structure, and final properties in metallic components [10]. Structural-interface studies further show that deposition strategy can influence microstructure and mechanical response in additively manufactured aluminium alloys [11]. Functionally graded WAAM examples illustrate how material transitions can be created through wire-based deposition [12]. Hybrid manufacturing research similarly shows that additive and forming steps can be combined to produce functional structural parts [13]. While in some cases, substrate is a transient part of fabrication, in other cases, the substrate is not removed at all.

The interface to be analyzed is hence considered as a local metallurgical transition phenomenon rather than as a geometrical interface. In the process of deposition, the first AA2319 layer partly melts the substrate surface, alloying the substrate material into the lower wall and forming an area having a microstructure different from both the initial substrate and the top deposited material. In addition, the substrate takes away the heat faster compared to the other layers of deposits and restricts the deformation of the lower deposited material. Later on, the subsequent passes heat up the earlier deposited material as well as the area near the substrate. Consequently, the formed transition layer consists of several zones namely: substrate not affected by heat, substrate affected by heat, partially molten material, melt zone, first layer of deposition, and top deposit.

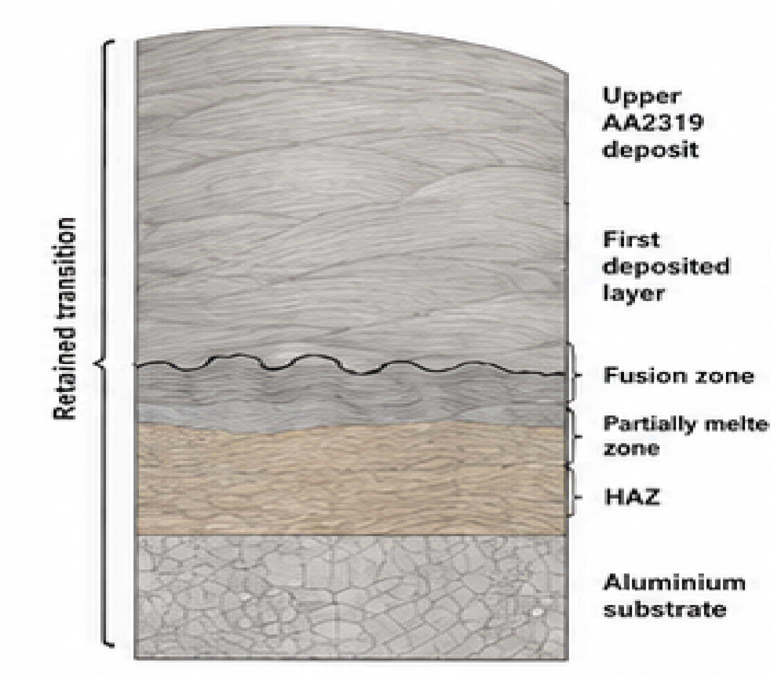

Figure 1: Retained interface zones.

The separation in Figure 1 is critical because each zone has control over a unique failure path. Substrate HAZ softening may occur, the partially melted zone may be susceptible to liquation, the fusion zone may have dilution-induced composition changes, the first deposition layer may have porosity, oxide cracking, or grain boundary cracks, and the top deposition layer will harden through aging. Friction-stir and related solid-state processing literature shows that severe local thermomechanical deformation can substantially alter aluminum microstructure [14]. Weld solidification studies explain why hot cracking and solidification-path effects remain important in fusion-based processing [15]. Partially melted zone cracking in AA6061 welds also shows why a retained substrate-side region may control failure [16]. Failure of all zones at once would overlook the significance of deposit-controlled tensile failure, failure at the fusion interface, a crack path within the lower wall, and strain localization within the substrate.

AA2319 is an aluminium filler alloy that contains Cu and is suitable for aluminium welding and additive deposition due to its compatibility with age-hardening treatments. The performance of AA2319 is greatly impacted by porosity, solidification properties, inter-pass deformation, and post deposition heat treatments. Inter-layer cold working has been reported to increase strength in additively manufactured Al–Cu alloys [17]. Porosity reduction has also been linked with inter-layer working and post-deposition heat treatment [18]. Rolling between layers can additionally influence residual stress and distortion in aluminium wire arc additive manufacture [19]. CMT based deposition processes have also been linked to the porosity and bead stability of aluminium alloys [20]. However, although these advantages are significant, they are not enough on their own to ensure interface integrity.

Selection of the substrate alloy brings about a change in the problem of interfaces. The combination of substrate material being a 2219-T8 alloy and AA2319 filler results in the presence of a common base material as well as similarities between the two alloys as far as the major alloying system is concerned. As such, this combination should minimize severe chemical discontinuity although failure could result from imperfections on the first layer, porosity, and fracture at the fusion boundary. A substrate made from a 2024-T3 alloy is one that has higher magnesium content than the AA2319 filler; hence, the deposition process will lead to Mg-containing dilution in the deposit. This will make the alloy more hardenable but may also form grain boundary areas that can easily crack and exhibit electrochemical contrast.

The significance of the retention of the interface is related to similar local parameters associated with failure mechanisms. Pitting corrosion in aluminum alloys is governed by local passive-film breakdown and chemistry at the attack site [21]. Aluminum pitting studies also emphasize the role of chloride exposure and surface heterogeneity [22]. Intermetallic phases can produce strong local electrochemical contrast in aluminum alloys [23]. S-phase particles and their surrounding regions can be particularly important in Al–Cu–Mg localized dissolution [24]. Temper condition can further change aluminum-alloy corrosion behaviour by modifying microstructure and local electrochemical response [25]. The presence of minor compositional gradients between grains or intermetallic precipitates in Cu-containing and Mg-alloyed aluminum alloys can lead to localized electrochemical processes. Cracking and porosity can entrap electrolyte and increase stress concentrations. Softening at the HAZ can result in accumulation of localized plastic deformation before yielding in the matrix. For these reasons, it is possible for both areas of mechanical weakness and susceptibility to corrosion to be located at the same point even in the absence of corrosion measurements.

The present study focuses on the characterization of AA2319 wire deposit weldments in 2219-T8, 2024-T3, traditional 6061-T6, and high velocity oxygen fuel 6061-T6 materials. The focus of this research is to establish the local region responsible for retaining the interface integrity. The methodology will include the use of tensile tests, microhardness analysis, optical microscopy, fractography using scanning electron microscopy, energy dispersive X-ray spectroscopy for chemical analysis, and digital image correlation for strain mapping. The focus here is to consider the influence of proof stress, ultimate tensile strength, elongation, hardness distribution, rupture location, and strain localization.

2. Materials and methods

The deposition of AA2319 aluminium wire was carried out on four substrates, namely 2219-T8, 2024-T3, conventional 6061-T6 and rapidly solidified 6061-T6. These substrate-alloy systems are named as 2219+2319, 2024+2319, rolled 6061+2319 and RSA-6061+2319. The rapidly solidified 6061-T6 was prepared through melt spinning, resulting in a finer structure than the conventionally rolled 6061-T6. Deposited wall lengths and height were roughly 200 mm and 50 mm, respectively. Interface tensile test specimens were machined such that the gauge section would pass through the substrate, heat affected zone, fusion zone and deposited AA2319 alloy. The thickness of the specimen at the interface area was roughly 2.5 mm.

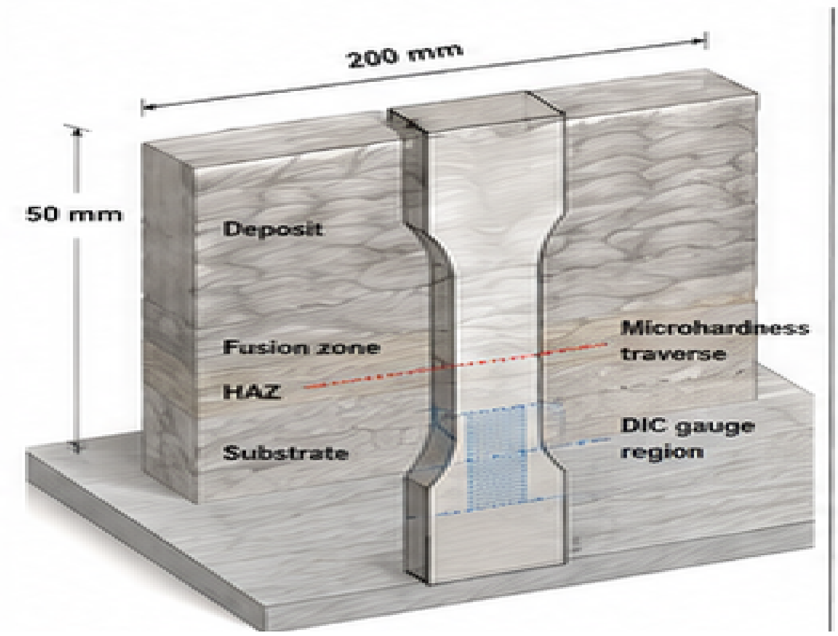

Figure 2: Coupon extraction geometry.

The specimen preparation procedure in Figure 2 plays an essential role in the analysis of the tension tests. The gauge portion includes the substrate, heat affected zone, weld metal, first-deposited layer of AA2319 alloy, and upper deposit, implying that the obtained results do not reflect the bulk-wall behavior. Failure may take place in the HAZ of the substrate, on the fusion interface, within the first layer of deposition, or in the upper wall.

Layer one was produced via pulsed cold metal transfer technique on the cold substrate. Layers two and above were built using CMT Pulse Advanced process route. Feed wire speed for layer one was 7 m min^{-1}; for layers two to three it was 9 m min^{-1}, for layers four to five – 7.5 m min^{-1}, and for layer six and beyond - 6 m min^{-1}. Travel speed was 10 mm s^{-1}, the standoff distance was 13 mm, shielding gas flow rate was 20 L min^{-1}, while the inter-layer dwell time was 120 s. Inter-pass rolling was done with a rolling diameter of 100 mm, a rolling force of 45 kN, and travel speed of 10 mm s^{-1}, approx. 30 s after the deposition. Heat treatment included solutionizing at 535°C for 90 min, followed by water quenching and ageing at 175°C for 3 h. These process routes and numerical conditions are summarized in Figure 3.

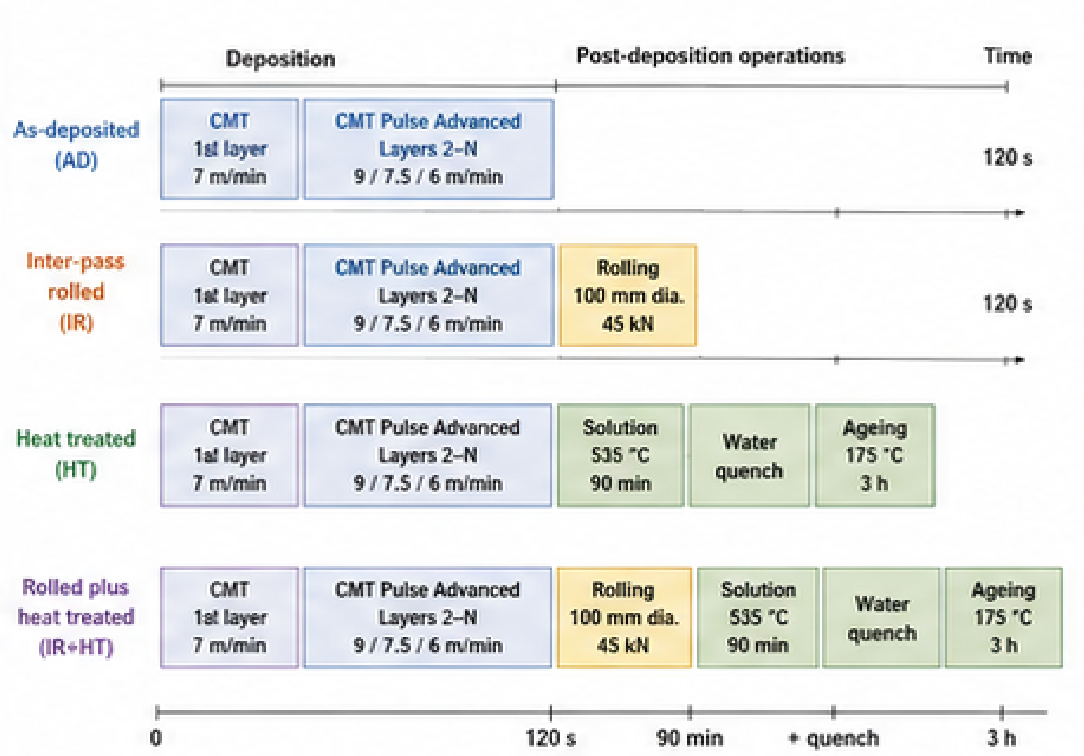

Figure 3: Processing conditions.

Four separate lines on Figure 3 indicate a difference between the two processes that occur under deformation and precipitation. Rolling was supposed to result in deformation of the deposited wall and decrease its susceptibility to defects. Since the first layers are subject to the limitations of the substrate, the reaction of the lower part of the wall could be different from that of the upper layer. Heating results in precipitation, which leads to strengthening of AA2319 but does not necessarily return the areas of the 6061-T6 substrate softened in the course of deposition. Rolling and heat treatment, thus, is not only an additively strengthening process but a process that changes defect structure, residual stresses, precipitates formation, and fracture sites simultaneously.

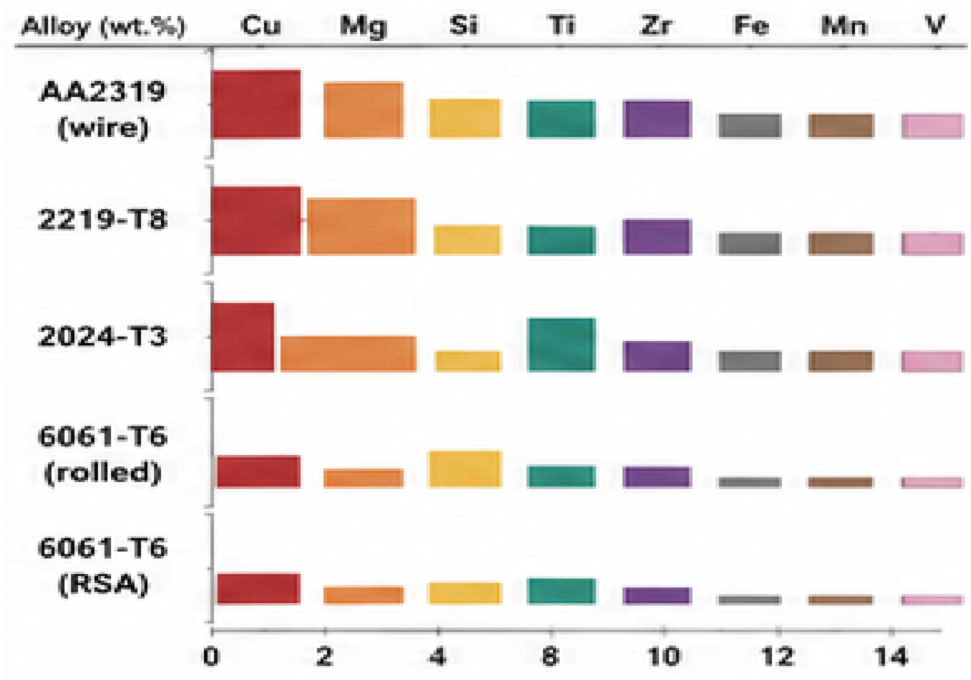

Figure 4: Alloy chemistry fingerprints.

Figure 4 shows the composition of the wire and substrates. AA2319 and 2219 have similar Cu-based compositions. However, 2024 differs by having more Mg, whereas 6061 brings Mg-Si precipitation sensitivity. These differences in chemistry can explain the different reactions of interfaces from the wire deposition. Specifically, 2219+2319 have a compositionally close combination; 2024+2319 has a combination of Mg-added lower composition wire; and 6061+2319 systems behave according to substrate properties in HAZ region.

The tensile samples were analyzed in accordance with ASTM B557M standard with a testing speed of 1 mm/min [26]. The reference coupons made of the substrate material and deposited area were employed as well as the samples with an interface layer for comparison purposes. The microhardness profile was conducted along the polished cross section with a load of 200 g for 15 sec. The metallographic samples as well as broken tensile specimens were polished and etched with Keller's solution. SEM examination of fracture surface and specific areas of the interface layer was carried out. The EDS analysis was conducted for studying the chemical composition of the interface layer. The 6061-based materials were examined using digital image correlation to evaluate strain localization in the substrate, HAZ, fusion line, and deposited regions.

3. Results

Each of the four substrate combinations had unique interfacial properties since each substrate affected the lower AA2319 deposit differently. The 2219-T8 substrate offered the closest chemical affinity for the AA2319 deposits. The addition of magnesium into the deposit by 2024-T3 substrate occurred in the first deposited region. A softening of the HAZ below the fusion line by the conventional rolled 6061-T6 substrate happened. The liquation effect was minimized in the rapidly solidified 6061 substrate. These differences are reflected in the tensile values, hardness profiles, fracture paths, and DIC strain fields.

Table 1: Metallurgical role of each retained-interface system.

Interface system	Local metallurgical condition	Expected mechanical response	Degradation-sensitive zone
2219+2319	Cu-rich substrate paired with Cu-rich AA2319 deposit	Deposit-controlled as-deposited strength and improved strength after heat treatment	First deposited layer and fusion boundary
2024+2319	Mg-bearing 2024 diluted into Cu-rich lower AA2319 deposit	Local hardening with low ductility when grain-boundary cracking develops	Mg-enriched lower deposited region
Rolled 6061+2319	Mg-Si strengthened substrate exposed to deposition thermal cycles	Substrate-side HAZ softening and strain localization below the fusion line	Softened substrate HAZ
RSA-6061+2319	Fine-grained rapidly solidified 6061 joined to AA2319	Reduced liquation severity and improved post-heat-treatment strength	Refined but still softened substrate-adjacent region

As shown by the differences illustrated in Table 1, the substrate plays an active role within the deposited layer. In the case of the 2219 substrate, the difference in composition is minimized, whereas the 2024 substrate alters the chemistry of the bottom deposited wall. The use of 6061 substrates results in a change in controlling weaknesses from the deposited AA2319 to the substrate. This variation explains why a single value such as proof stress is not sufficient for interface acceptance.

3.1 Overall tensile behaviour

The primary tensile results are tabulated in Table 2 and plotted in Figure 5. As-deposited 2219+2319 interface had proof stress of 118 ± 8 MPa, ultimate tensile strength of 257 ± 13 MPa, and elongation of 8.5 ± 1.5%. Rolling resulted in higher proof stress of 224 ± 21 MPa, while elongation was only 2.2 ± 0.7%. With heat treatment, the strength was increased even further, resulting in rolled and heat treated samples having proof stress of 272 ± 22 MPa and UTS of 362 ± 26 MPa. The as-deposited 2024+2319 interface had proof stress of 147 ± 14 MPa, UTS of 232 ± 12 MPa, and elongation of 2.8 ± 0.9%. Although the proof stress for the rolled 2024+2319 alloy was 248 ± 17 MPa and UTS was 270 ± 18 MPa, elongation was 2.2 ± 0.7%. The 6061-based systems showed lower proof stresses than the strongest 2xxx-based conditions but much larger elongation after heat treatment.

Table 2: Tensile properties and controlling fracture behaviour of AA2319 retained interfaces.

Interface system	Condition	Proof stress (MPa)	UTS (MPa)	Elongation (%)	Controlling behaviour
2219+2319	As-deposited	118 ± 8	257 ± 13	8.5 ± 1.5	Strength followed the softer AA2319 deposit
2219+2319	Inter-pass rolled	224 ± 21	270 ± 18	2.2 ± 0.7	Strength rose but ductility decreased sharply
2219+2319	Heat treated	270 ± 18	355 ± 12	3.5 ± 0.7	High strength with fusion-boundary fracture
2219+2319	Rolled + heat treated	272 ± 22	362 ± 26	4.0 ± 2.0	Fracture shifted away from the fusion boundary
2024+2319	As-deposited	147 ± 14	232 ± 12	2.8 ± 0.9	Lower-wall cracking limited ductility
2024+2319	Inter-pass rolled	248 ± 17	270 ± 18	2.2 ± 0.7	Crack visibility decreased but ductility stayed low
Rolled 6061+2319	As-deposited	124 ± 21	208 ± 18	5.9 ± 2.6	Softened substrate HAZ controlled failure
Rolled 6061+2319	Heat treated	168 ± 7	280 ± 2	20.0 ± 0.2	High elongation with substrate-side strain bias
RSA-6061+2319	As-deposited	148 ± 18	225 ± 10	6.9 ± 1.8	Improved strength relative to rolled 6061
RSA-6061+2319	Heat treated	209 ± 12	328 ± 7	16.6 ± 1.1	Best 6061-based strength and strain balance

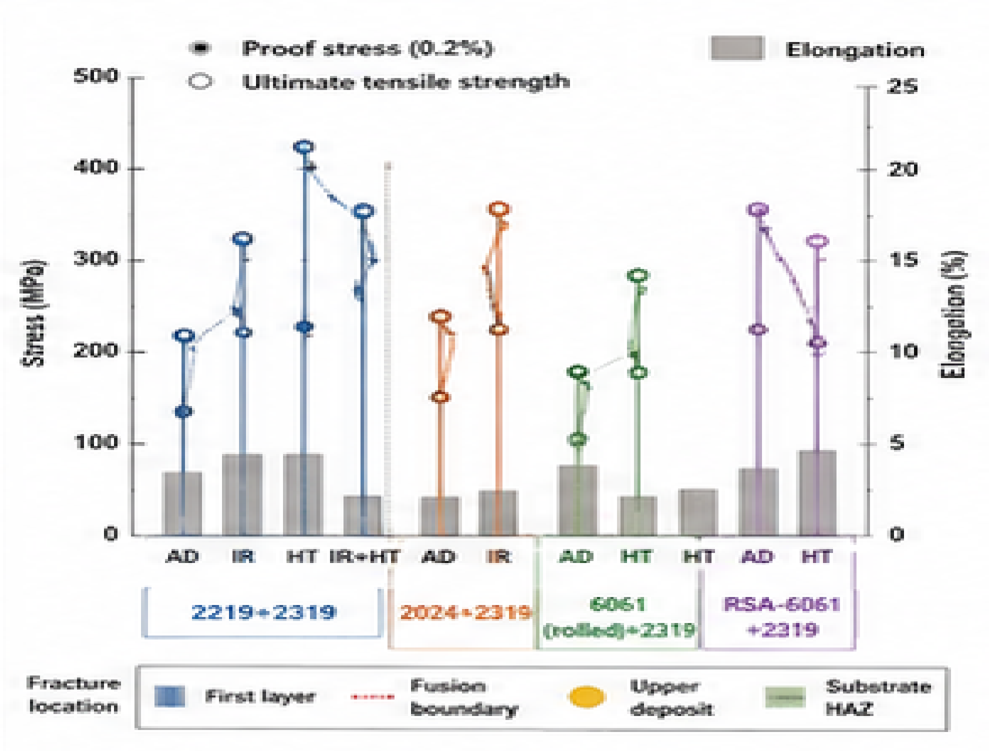

Figure 5: Strength, ductility, and fracture zone.

The "integrated property domain" illustrated in Figure 5 allows for separating the concepts of strength and damage tolerance. Both the rolled 2024+2319 alloy and the rolled 2219+2319 alloy had relatively high proof strength; however, in both cases, very low elongations were noted. On the contrary, the heat-treated specimens based on the 6061 alloy demonstrated quite the opposite trends: their proof strength was not high, while their elongation was relatively high compared to other conditions.

3.2 2219+2319 Interface

The 2219+2319 interface demonstrated the highest compatibility among the materials used. In its native state, the proof stress and UTS were similar to those exhibited by the AA2319 deposit; hence, the interface had a lower proof stress and UTS as compared to those of the AA2319 deposit. The values of 118 $\pm$ 8 MPa for proof stress and 257 $\pm$ 13 MPa for UTS were more reflective of the dominant properties of the deposit as opposed to interface failure. However, the elongation of 8.5 $\pm$ 1.5% was less than that of the AA2319 deposit (15.5%).

The hardness gradient between the as-deposited layers of 2219+2319 was characterized by a step change from the harder substrate of 2219 to the softer AA2319 deposit. The hardness for the substrate layer was roughly 90 HV, whereas that for the deposit next to the fusion line was roughly 70 HV. In view of this difference in hardness, it can be understood that the deposit dominated plasticity; however, there is evidence from the results of this hardness gradient that the transition was mechanically inhomogeneous. Interpass rolling helped increase the hardness of the deposit as well as the fusion area, although the fusion zone was still relatively softer than the upper wall. The combined hardness and fracture behaviour are presented in Figure 6.

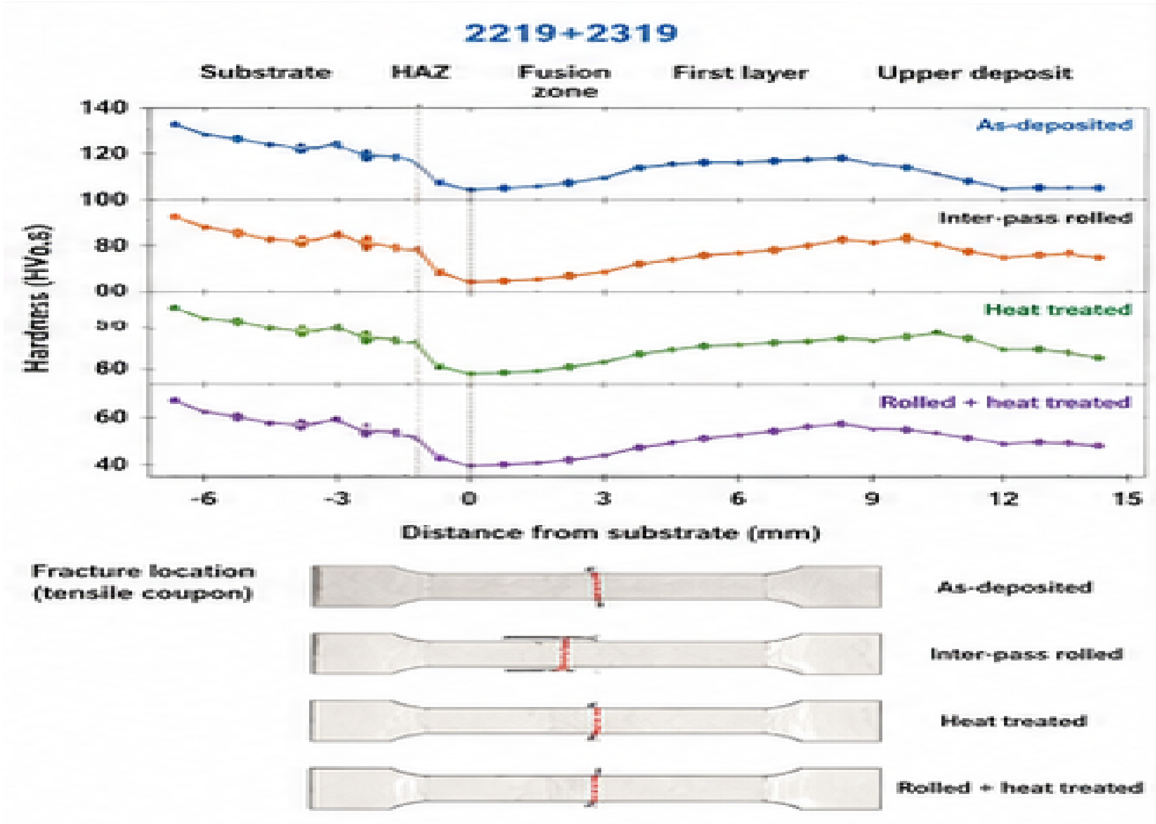

Figure 6: 2219+2319 transition response.

In Figure 6, the answer to why the rolled and heat-treated state is more compelling than both the rolling and the heat treatments individually is provided. With rolling, proof stress was enhanced from 118 ± 8 MPa to 224 ± 21 MPa while elongation reduced from 8.5 ± 1.5% to 2.2 ± 0.7%. In this case, the rise in proof stress did not correspond to increased interface compatibility. The very small elongation shows that the potential for deformation was reached early because the initial deposition site still had defects or strain incompatibility issues.

Heat treatment increased the strength of 2219+2319 to a great extent. In the case of heat treatment, the proof stress was 270 ± 18 MPa and ultimate tensile strength (UTS) was 355 ± 12 MPa. In the case of roll plus heat treatment, the proof stress was 272 ± 22 MPa and UTS was 362 ± 26 MPa. The main distinguishing factor between the two cases can be explained by the point of fracture. The point of fracture for heat treatment was located on the fusion line, thus revealing the presence of localized fracture.

The 2219 + 2319 combination proves that compatibility between alloys is good for the initial state, but does not make interface qualification unnecessary. What makes an ideal combination is not only its high proof stress; rather, it is the combination's high strength and its ability to create a fracture that does not break the fusion line. In the case of retained substrate configurations, this shift in the pattern of fracture becomes more important than a marginal increase in the UTS because the interface endures the tensile test.

3.3 2024+2319 interface

The fusion zone formed in the 2024+2319 interface had a tougher composition due to the magnesium in the substrate alloy diffusing into the deposited layer in the lower AA2319 deposit. The fusion zone had a hardness of about 99 HV while that in the 2219+2319 interfaces was about 68 HV. This was a chemical expectation since the lower alloy was not an Al-Cu based alloy anymore; it now had magnesium alloy enrichment and consequently reacted differently with precipitation. The coupling between Mg enrichment, hardness, and the lower deposited region is shown in Figure 7.

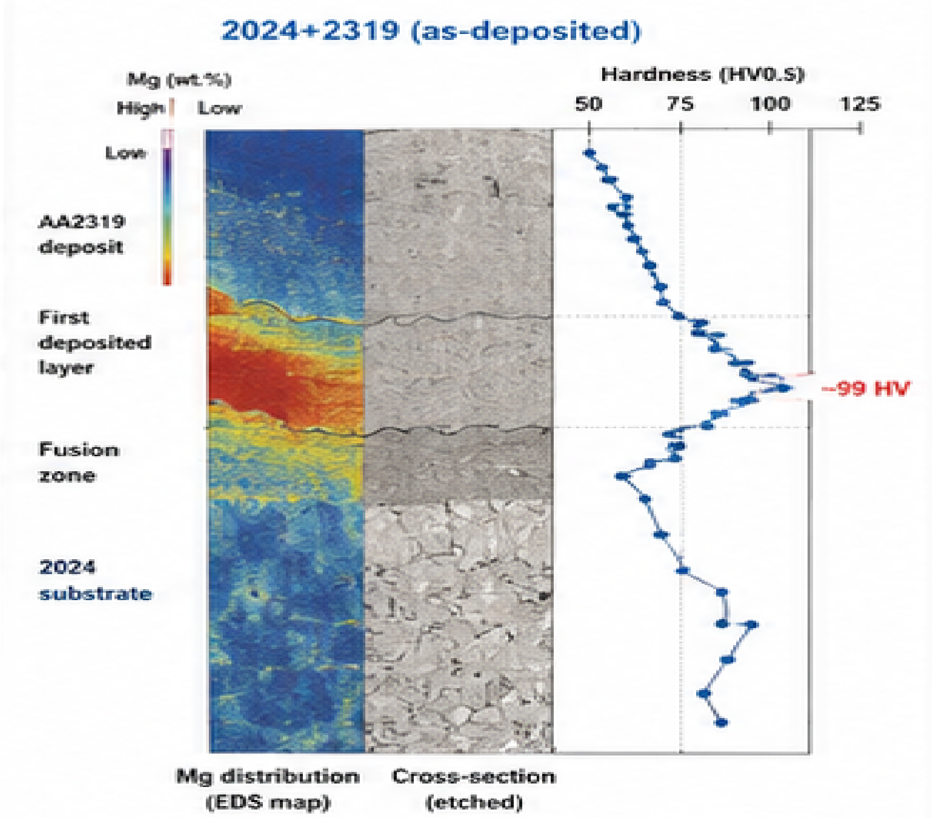

Figure 7: Mg-modified lower wall.

The hardness map and hardness trace presented in Figure 7 prove that this interface can't be evaluated based on its hardness value only. The 2024+2319 interface obtained from as-deposited process showed the yield strength of 147 ± 14 MPa, which is higher than the as-deposited 2219+2319 yield strength. It had a UTS of 232 ± 12 MPa, while elongation was equal to 2.8 ± 0.9%. The fracture happened at the transition point between the first layer and second layer deposition. The lower wall was therefore locally strong but crack-sensitive. Hardness alone gave an incomplete impression of interface quality.

The fracture morphology comparison in Figure 8 reveals that inter-pass rolling enhanced the load-bearing capability of the 2024+2319 specimens without restoring the ductility. The proof stress rose up to 248 ± 17 MPa, and the UTS rose to 270 ± 18 MPa. At the same time, rolling relocated the fracture surface away from the first bead and eliminated any observable cracks. Nevertheless, the elongation was still very low at 2.2 ± 0.7%. The lack of any considerable improvement in the elongation suggests that rolling altered the fracture characteristics but did not eliminate the limiting factor of the strain tolerance.

The 2024+2319 interface is considered to have the greatest risk of degradation compared to other investigated interfaces due to the fact that it has both mechanical and chemical alterations in its weaker area. Redistribution of magnesium and copper may lead to the enhancement of electrochemical gradients locally, whereas cracks along grain boundaries may hold an electrolyte solution and apply local stress. S-phase particles and their vicinity have been identified as initiators of localized corrosion for aluminum-copper-magnesium alloys [24]. Intermetallic-phase electrochemistry further supports the importance of local galvanic contrast in such alloys [23]. The above results do not give the corrosion rates, but it is clear that the lower deposited area is better suited for localized electrochemical and corrosion-fatigue studies.

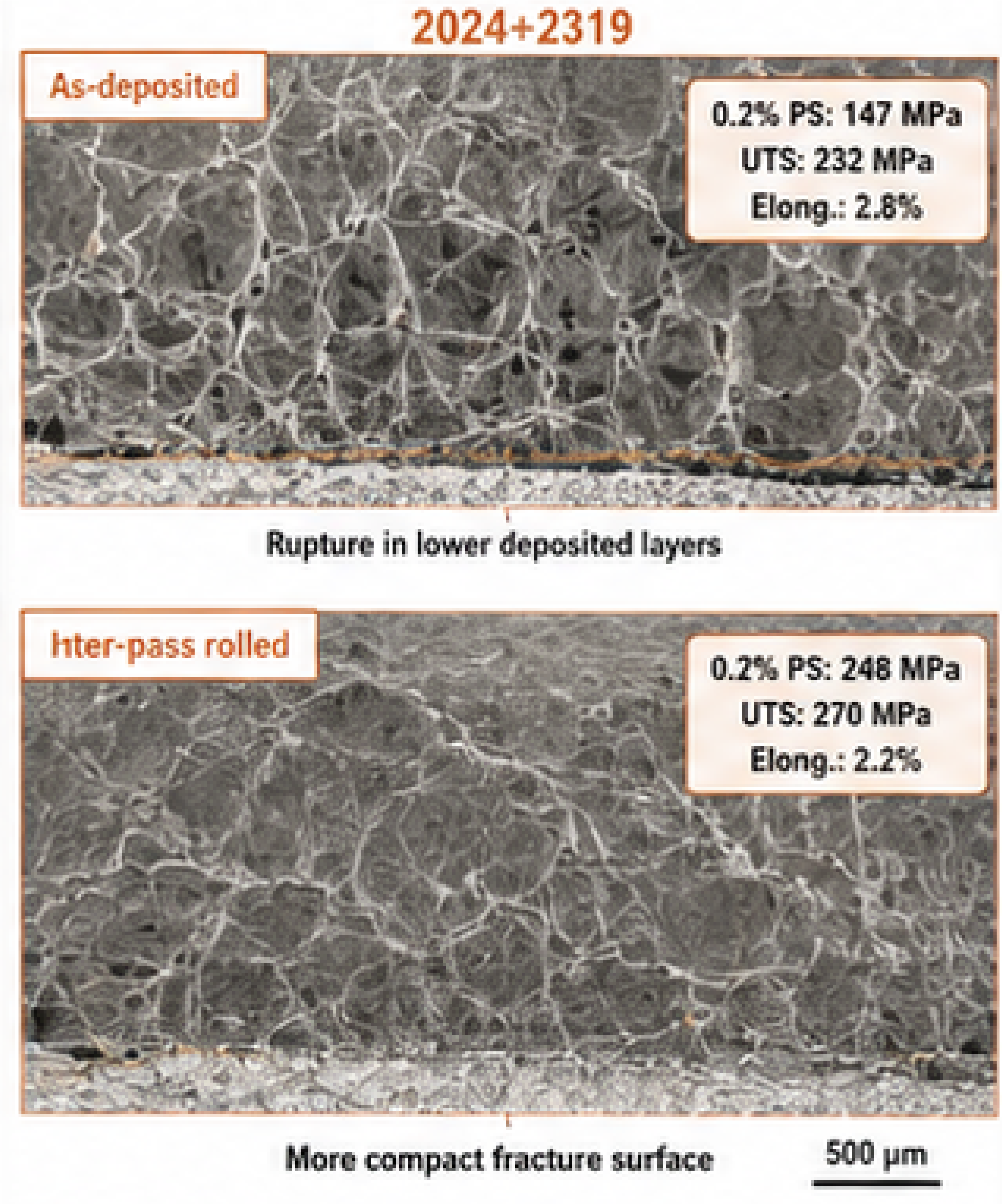

Figure 8: 2024+2319 fracture contrast.

3.4 6061-based joints

For the rolled joint of 6061+2319, the softening of HAZ on the substrate side was dominant. The proof stress for the as-deposited sample was measured at 124 ± 21 MPa; the ultimate tensile strength was 208 ± 18 MPa and elongation was 5.9 ± 2.6%. It is seen from the hardness map that there was a significant drop in the HAZ of the 6061 substrate below the fusion line. The lowest hardness value was found in the HAZ rather than in the 2319 aluminum deposit. Aluminium-welding literature describes the heat sensitivity of precipitation-hardened alloys [4]. Partially melted zone and HAZ cracking studies likewise show why AA6061 weld regions can be locally weak [16]. The HAZ softening valley in rolled 6061+2319 is shown in Figure 9.

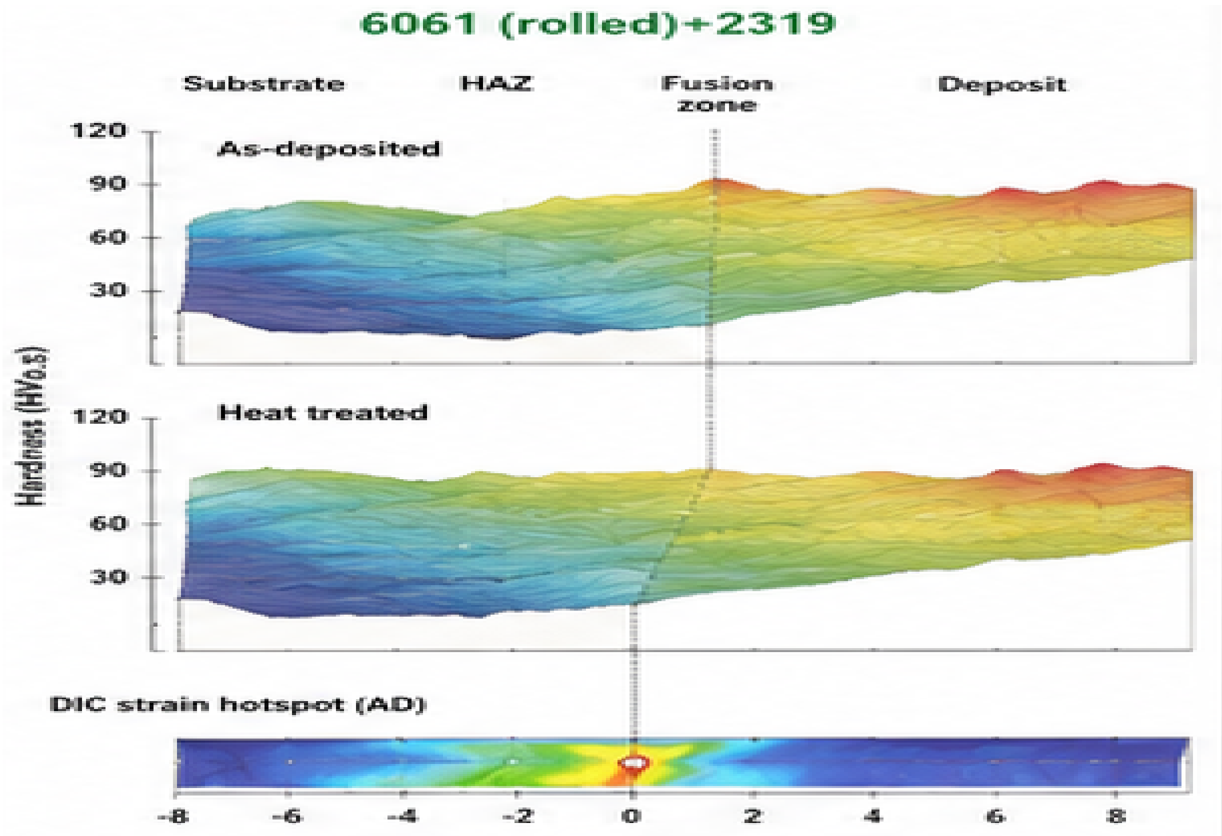

Figure 9: Rolled 6061 HAZ softening.

The hardness map from the terrain style shown in Figure 9 suggests that the critical zone must be situated beneath the melting line. Heat treatment enhanced the overall performance of the rolled 6061+2319 alloy in terms of tensile testing, as the proof stress reached 168 ± 7 MPa, the UTS rose to 280 ± 2 MPa, and elongation amounted to 20.0 ± 0.2%. The high elongation ratio means that this material could endure massive deformations. Yet, the strain distribution still favored the substrate side. In other words, the heat treatment did not restore the 6061 substrate fully back to T6 state, whereas the AA2319 deposit became stronger. The resulting interface was ductile but mechanically asymmetric.

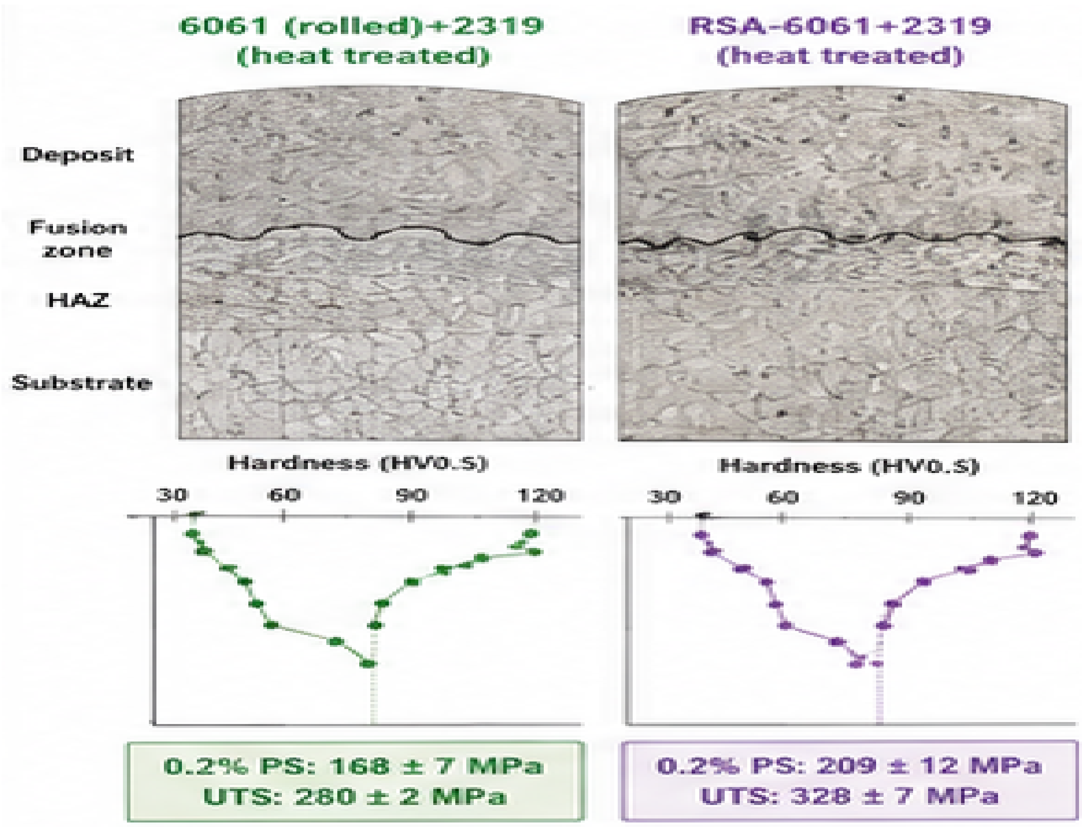

Figure 10: Refined 6061 interface response.

Interface analysis in the case of the RSA-6061+2319 alloy revealed the influence of the state of the substrate prior to deposition on the properties of the retained interface. The as-deposited RSA-6061+2319 alloy displayed a proof stress of 148 ± 18 MPa and ultimate tensile strength of 225 ± 10 MPa, which were higher compared to the similar values for the rolled material of 6061+2319. Elongation in the RSA alloy was measured at 6.9 ± 1.8%, slightly higher than that for the rolled alloy 6061+2319 as-deposited condition.There was still softening of the heat-affected zone, however. However, the liquation was less severe compared with conventionally rolled 6061. The heat treatment comparison between rolled and rapidly solidified samples is given in Figure 10.

Based on the comparison provided in Figure 10, it can be seen that the heat treated RSA-6061+2319 system had the highest performance level compared to other 6061 alloys. In this case, the proof stress was measured to be 209 ± 12 MPa, while the UTS was 328 ± 7 MPa, and the elongation value was as high as 16.6 ± 1.1%. Despite the fact that in this case the substrate-side HAZ was not eliminated, the optimization of the substrate resulted in less liquation and better strength-strain performance.

3.5 Localization of DIC strain in 6061-based samples

The results of the DIC analysis proved the assumption regarding the hardness of the 6061-based samples correct. The strain localization took place at a distance of around 3-4 mm from the fusion line in the as-deposited rolled 6061+2319 sample. The rupture happened in the softened HAZ zone. The AA2319 filler metal had no role in controlling failure despite being present in the gauge section. The softened HAZ on the substrate side was the sink of deformation.

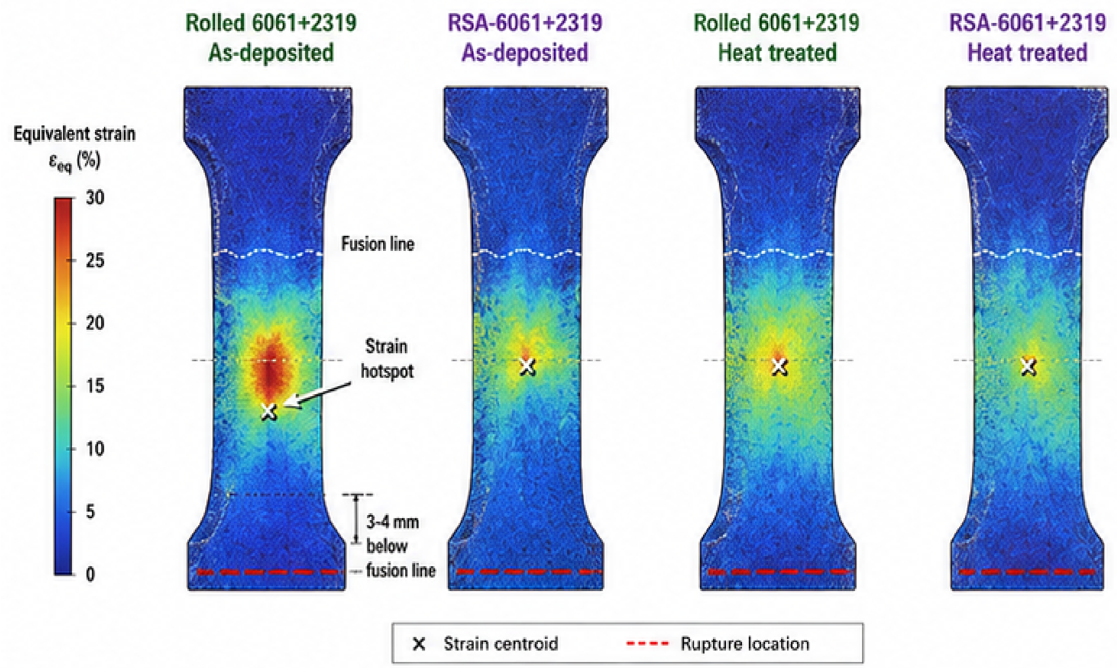

Figure 11: 6061 strain localization.

The strain maps shown in Figure 11 revealed that while rapid solidification influenced the deformation pattern of the alloy, the concentration bias on the substrate side did not get eliminated entirely due to rapid solidification. Though the localization of RSA-6061 field after deposition occurred in the substrate HAZ, it showed lesser localization compared to that of rolled 6061. Heat treated rolled 6061+2319 exhibited substrate biasing, whereas heat treated RSA-6061+2319 had distributed strains.

4. Discussion

As evident from the measurements, AA2319 deposit failure depends on the substrate involved in the interface. In case of the 2219+2319 interface, first layer and fusion boundaries determine its strength while the 2024+2319 interface is defined by cracking at the Mg-alloyed low wall. In contrast, HAZ softening of the substrate determines the strength of the 6061-based alloys' interfaces.

The reaction between the 2219+2319 samples demonstrates the importance of chemical compatibility. As can be seen from the results, the as-deposited sample had lower strength than the second deposit; it appears that the presence of copper in the substrate mitigated the harmful effects of dilution. Nevertheless, decreased elongation and inferior ductility of the rolled sample prove that chemical compatibility alone does not assure positive results. The initial deposit is still prone to mechanical treatment and defects, as well as stress concentration. The combination of high strength and fracture within the upper deposit is characteristic of the rolled-and-heat treated sample.

From the analysis of the 2024+2319 case, one can deduce that the local hardening effect should be considered with great care. The alloying by magnesium of the fusion zone increased its hardness compared to the 2219+2319 counterpart; however, the lower wall displayed extremely low elongation to fracture. Local dissolution studies of S-phase particles explain why Al–Cu–Mg regions may be chemically vulnerable [24]. Light-alloy metallurgy further shows why strengthening and fracture resistance must be interpreted with alloy family and microstructural state [3]. The problem does not consist of adding magnesium per se, but the highly localized change in the chemistry as a result of mixing of the first AA2319 melt with the base material. It is formed during the first phase of sedimentation, which is characterized by thermal constraints in addition to solid structure formation, re-heating, and strain. The hardened wall has high hardness as well as low fracture resistance.

It is clear from the examples of 6061 alloy-based interfaces that sometimes the substrate controls the failure despite the fact that the deposit material remains the same. Heat-treated precipitation-hardening 6061-T6 becomes weaker when the precipitation state of Mg-Si is affected due to welding or deposition processes [4]. Partially melted zone cracking in AA6061 welds gives a related example of substrate-side sensitivity [16]. The hardness decrease at the interface area and DIC strain peaks occurring there help to understand the mechanism of failure. It is possible to strengthen the AA2319 deposit via heat treatment; however, it does not return 6061 HAZ to its original condition. As a result, heat treatment can create a stronger deposit next to a softer substrate region.

The interface-zone correlation illustrated in Figure 12 then interprets such measurements into a picture of local control. It suggests that high proof stress is important only if it correlates with an adequate elongation and a non-fatal fracture point location. The 2219+2319 material combination represents an upper-deposit failure, not fusion boundary failure. 2024+2319 material combinations are linked to the Mg-enhanced lower wall region. All six cases involving 6061 are linked to the softened HAZ, except for RSA-6061+2319.

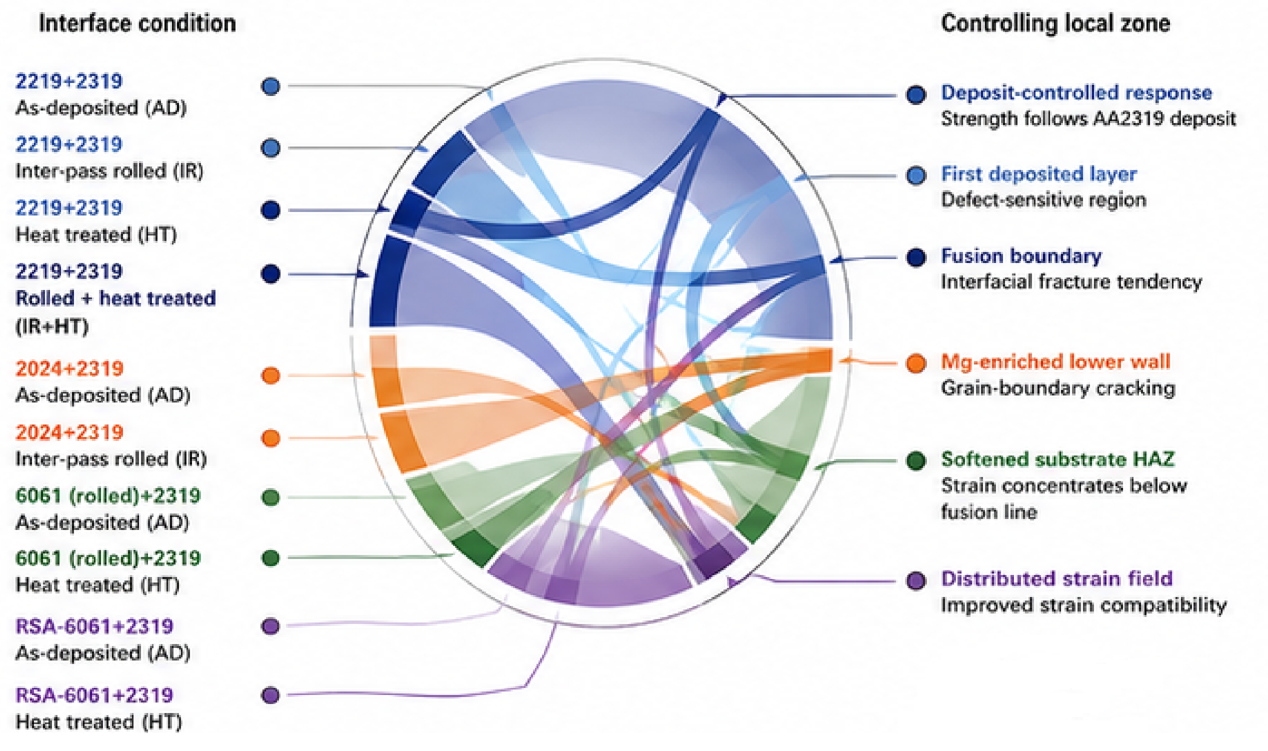

Figure 12: Controlling interface zones.

Rapidly Solidified 6061 is important since it illustrates how the condition of the substrate influences the behavior of the interface. While following the HAZ-controlled path, RSA-6061 coupons had higher strengths and distributed strains. This demonstrates that the substrate grain structure and its liquation properties must be specified for retained-substrate deposition cases. When designing components using the method, usually the substrate is considered to be a plate of an alloy temper. However, the current experimental results prove that it makes a difference whether or not the substrate is taken into account.

The analysis of tensile performance further demonstrates that proof stress alone cannot be used as the sole criterion for acceptance. Both rolled 2024+2319 and rolled 2219+2319 materials possessed high proof stress but elongation at less than 2%. Such results could seem favorable in terms of only material strength, while they were not when it came to fracture toughness. On the other hand, both heat treated rolled 6061+2319 and heat treated RSA-6061+2319 samples had a significantly higher value of elongation but still had strain field affected by substrate HAZ. The best balance of conditions was obtained for roll-and-heat treated 2219+2319 due to the combination of high strengths and fracture outside the retained zone.

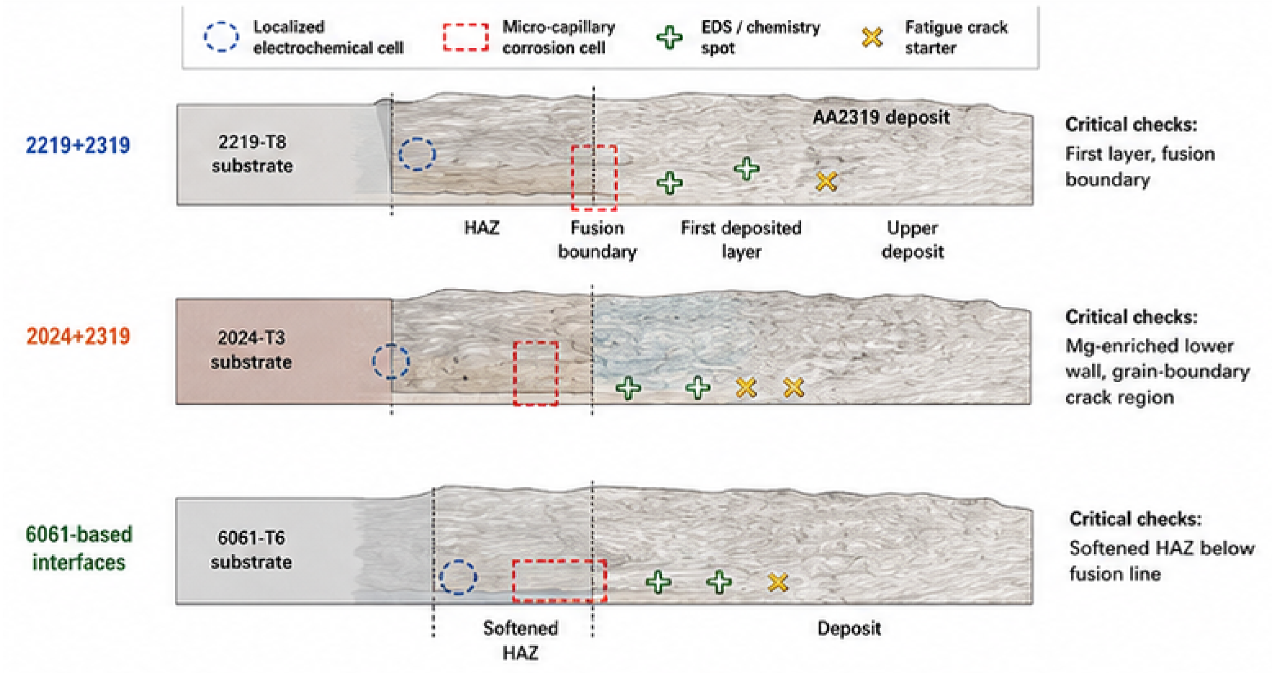

Figure 13: Local durability test sites.

Any corrosion-related discussion must necessarily be constrained by the data obtained. Polarization tests, electrochemical impedance spectroscopy, immersion tests, salt spray test, and corrosion fatigue crack growth rate measurements have not been performed. Nevertheless, the obtained data allow us to determine the sites of interest. For 2219+2319, it should be the fusion line and first deposited layer. For 2024+2319, it should be Mg-containing lower wall and grain boundary cracked site. In turn, for all 6061-based interfaces, it is the substrate softening heat affected zone under the influence of cyclic deformation and chloride stress. Aluminum-alloy durability is governed by localized pitting features that may be highly sensitive to small chemical and mechanical differences [21]. Pitting studies confirm that chloride-driven attack can be localized rather than coupon-average controlled [22]. Intermetallic-phase electrochemistry further supports the need to test chemically distinct local regions [23]. Durability test locations are shown in Figure 13.

It can be seen from Figure 13, which gives an indication for testing sites, that future corrosion and fatigue tests will have to focus on localized regions rather than the entire coupon. This is because the first deposited layer/fusion zone in 2219+2319, the Mg-rich lower wall region in 2024+2319, and the heat affected zone in 6061 alloys will remain confined spatially. Therefore, exposing the entire coupon surface may not yield results for those specific regions.

Practically speaking, retention of substrate for aluminium wire deposition would need zone-specific qualification. The required interface should have high strength, adequate elongation, a moderate increase in hardness, no crack sensitive structures on the lower wall side, and a fracture location other than at the fusion line. In case DIC results are available, there must be no collapse of strain into a localized soft zone. The selection criterion is shown in Figure 14.

According to the table presented in Figure 14, the optimal retained interfacial material system is the heat treatment of rolled 2219+2319, which provides the highest proof stress of 272 ± 22 MPa and ultimate tensile stress of 362 ± 26 MPa, with no fracture through the fusion interface. Heat-treated RSA-6061+2319 becomes the most optimal condition for 6061 alloy, since its mechanical properties have been improved and more uniform strain distribution can be achieved, although HAZ characteristics remain critical. The 2024+2319 situation needs attention as there is a combination of local strengthening with low ductility and increased susceptibility to wall cracks.

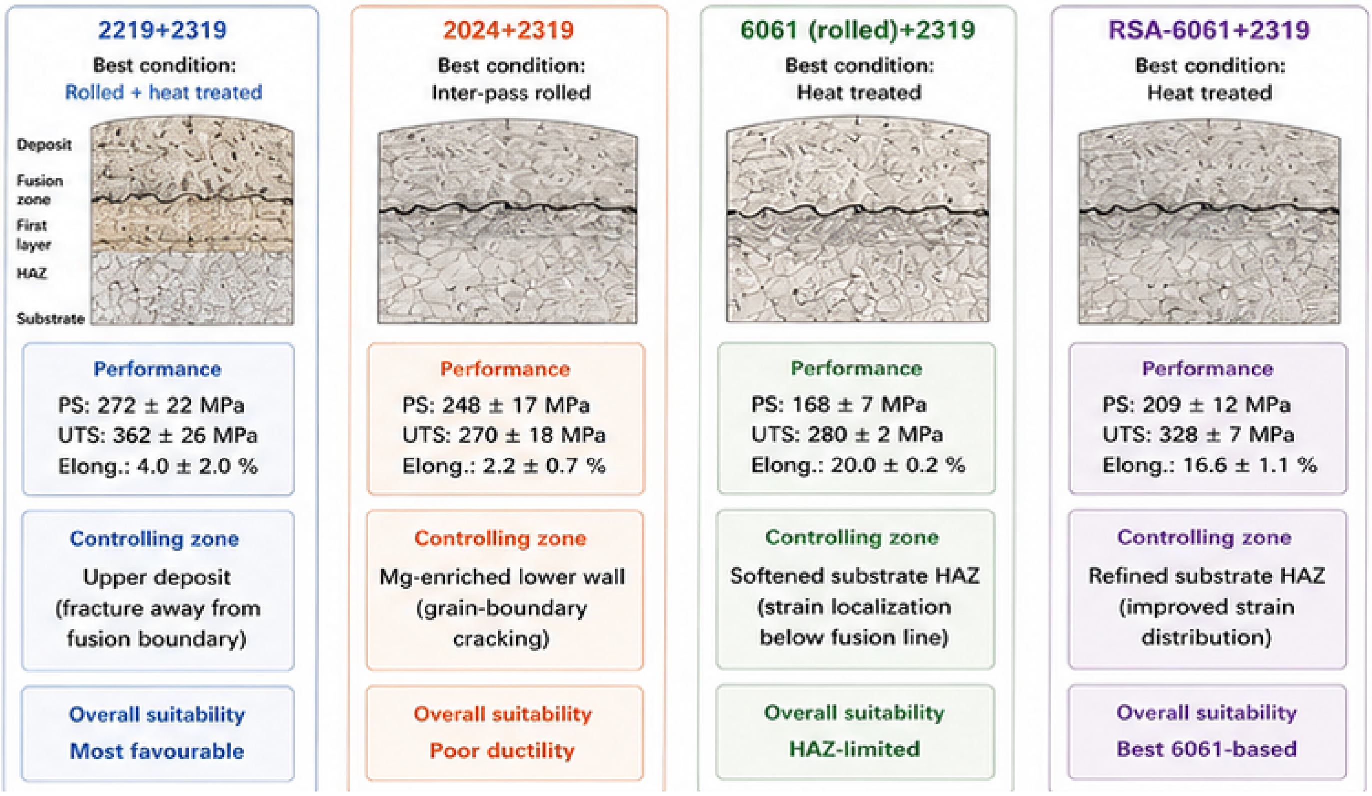

Figure 14: Interface selection summary.

5. Conclusions

Interfaces formed by the retention of the AA2319 wire using DED are dominated by the local fracture mechanisms and not the overall mechanical properties of the deposit. This will be dependent on the alloy of the substrate as well as the process parameter setting. In 2219+2319, the key aspect lies in the first deposited layer and the fusion zone. In 2024+2319, the critical failure mechanism is the magnesium-containing lower part of the deposit. For 6061-series alloys, failure depends on the annealed HAZ on the substrate side of the fusion line.

The 2219+2319 combination had the best response in terms of rolling and heat treatment. The rolled and heat treated alloy attained a proof strength of 272 ± 22 MPa and ultimate tensile strength of 362 ± 26 MPa, and failed at a distance from the fusion line. The fracture offset means that the retained fusion line was not the preferred point of failure.

2024+2319 showed that an increase in hardness of the fusion zone does not guarantee integrity of the interface. Hardness was improved due to the addition of magnesium, reaching about 99 HV; however, low elongation was observed in the deposited layer wall, together with high sensitivity to grain boundary cracking. This area can be described as the most difficult transition area between the alloys under investigation.

Rolled interface between 6061+2319 is formed via HAZ softening underneath the fusion line. Heat treatment enhanced the elongation up to 20.0 ± 0.2%, while the strain was still localized on the substrate side. The addition of 2319 to RSA-6061 enhanced the properties of alloy 6061. It resulted in 209 ± 12 MPa proof stress, 328 ± 7 MPa ultimate tensile strength, and elongation up to 16.6 ± 1.1%. elongation, with a more distributed strain field than conventionally rolled 6061.

The most accurate choice of interface retention will be based on the combination of the following factors: strength, elongation, hardness profile, fracture location, local composition, and strain distribution by DIC. Corrosion testing has not been done directly, so any claims about corrosion should be restricted to identifying the degradation susceptible zones only. Further research will focus on conducting such tests as well as others mentioned above in these zones.

Conflict of interest

The author declares no conflict of interest.

References

[1] Davis, J. R. (1993). Aluminum and aluminum alloys. ASM international.
[2] Starke Jr, E. A., & Staley, J. T. (1996). Application of modern aluminum alloys to aircraft. Progress in aerospace sciences, 32(2-3), 131-172.

[3] Polmear, I., StJohn, D., Nie, J. F., & Qian, M. (2017). Light alloys: metallurgy of the light metals. Butterworth-Heinemann.
[4] Mathers, G. (2002). The welding of aluminium and its alloys. Elsevier.
[5] Wilson, D. M. (2019). Metallurgical and mechanical property characterization of additively manufactured 304L stainless steel. Colorado School of Mines.
[6] Williams, S. W., Martina, F., Addison, A. C., Ding, J., Pardal, G., & Colegrove, P. (2016). Wire+ arc additive manufacturing. Materials science and technology, 32(7), 641-647.
[7] Ding, J., Colegrove, P., Martina, F., Williams, S., Wiktorowicz, R., & Palt, M. R. (2015). Development of a laminar flow local shielding device for wire+ arc additive manufacture. Journal of Materials Processing Technology, 226, 99-105.
[8] Lockett, H., Ding, J., Williams, S., & Martina, F. (2017). Design for Wire+ Arc Additive Manufacture: design rules and build orientation selection. Journal of Engineering Design, 28(7-9), 568-598.
[9] Derekar, K. S. (2018). A review of wire arc additive manufacturing and advances in wire arc additive manufacturing of aluminium. Materials science and technology, 34(8), 895-916.
[10] DebRoy, T., Wei, H. L., Zuback, J. S., Mukherjee, T., Elmer, J. W., Milewski, J. O., ... & Zhang, W. (2018). Additive manufacturing of metallic components–process, structure and properties. Progress in materials science, 92, 112-224.
[11] Gu, J., Yang, S., Gao, M., Bai, J., & Liu, K. (2020). Influence of deposition strategy of structural interface on microstructures and mechanical properties of additively manufactured Al alloy. Additive Manufacturing, 34, 101370.
[12] Marinelli, G., Martina, F., Lewtas, H., Hancock, D., Ganguly, S., & Williams, S. (2019). Functionally graded structures of refractory metals by wire arc additive manufacturing. Science and Technology of Welding and Joining, 24(5), 495-503.
[13] Merklein, M., Schulte, R., & Papke, T. (2021). An innovative process combination of additive manufacturing and sheet bulk metal forming for manufacturing a functional hybrid part. Journal of Materials Processing Technology, 291, 117032.
[14] Mishra, R. S., & Ma, D. Z. (2005). Friction stir welding and processing. Materials science and engineering: R: reports, 50(1-2), 1-78.
[15] Cross, C. E. (2005). On the origin of weld solidification cracking. In Hot cracking phenomena in welds (pp. 3-18). Berlin, Heidelberg: Springer Berlin Heidelberg.
[16] Rao, K. P., Ramanaiah, N., & Viswanathan, N. (2008). Partially melted zone cracking in AA6061 welds. Materials & design, 29(1), 179-186.
[17] Gu, J., Ding, J., Williams, S. W., Gu, H., Bai, J., Zhai, Y., & Ma, P. (2016). The strengthening effect of inter-layer cold working and post-deposition heat treatment on the additively manufactured Al–6.3 Cu alloy. Materials Science and Engineering: A, 651, 18-26.
[18] Gu, J., Ding, J., Williams, S. W., Gu, H., Ma, P., & Zhai, Y. (2016). The effect of inter-layer cold working and post-deposition heat treatment on porosity in additively manufactured aluminum alloys. Journal of materials processing technology, 230, 26-34.
[19] Hönnige, J. R., Colegrove, P. A., Ganguly, S., Eimer, E., Kabra, S., & Williams, S. (2018). Control of residual stress and distortion in aluminium wire+ arc additive manufacture with rolling. Additive Manufacturing, 22, 775-783.
[20] Cong, B., Ding, J., & Williams, S. (2015). Effect of arc mode in cold metal transfer process on porosity of additively manufactured Al-6.3% Cu alloy. The International Journal of Advanced Manufacturing Technology, 76(9), 1593-1606.
[21] Frankel, G. S. (1998). Pitting corrosion of metals: a review of the critical factors. Journal of the Electrochemical society, 145(6), 2186-2198.
[22] Szklarska-Smialowska, Z. (1999). Pitting corrosion of aluminum. Corrosion science, 41(9), 1743-1767.
[23] Birbilis, N., & Buchheit, R. G. (2005). Electrochemical characteristics of intermetallic phases in aluminum alloys: an experimental survey and discussion. Journal of the Electrochemical Society, 152(4), B140-B151.
[24] Buchheit, R. G., Grant, R. P., Hlava, P. F., Mckenzie, B., & Zender, G. L. (1997). Local dissolution phenomena associated with S phase (Al2CuMg) particles in aluminum alloy 2024-T3. Journal of the electrochemical society, 144(8), 2621-2628.
[25] Andreatta, F., Terryn, H., & De Wit, J. H. W. (2004). Corrosion behaviour of different tempers of AA7075 aluminium alloy. Electrochimica acta, 49(17-18), 2851-2862.
[26] Standard, A. S. T. M. (2015). B557-15; Standard Test Methods for Tension Testing Wrought and Cast Aluminum-and Magnesium-Alloy Products. ASTM International: West Conshohocken, PA, USA.